Egypt. J. Chem. **Vol.** 64, No. 11, pp. 6137 - 6145 (2021)

Egyptian Journal of Chemistry

http://ejchem.journals.ekb.eg/

Cibacron red dye removal in aqueous solution using Synthesized $CuNiFe_2O_5$ Nanocomposite: Thermodynamic and kinetic studies

Amal Fadhil Kamil[1], Hussein Ismail Abdullah[1], Ahmed Mahdi Rheima[2*], Srwa Hashim Mohammed[3]

[1] *Department of Chemistry, College of Science, Mustansiriyah University, Baghdad, Iraq*
[2] *Department of Chemistry, College of Science, University of Wasit, kut, Iraq*
[3] *Department of Chemistry, College of education, University of garmian, kalar, Iraq*

Abstract

Dyes pollution is a major problem in the water, especially since the main factor is textile factories. The treatments for this problem through nanomaterials have taken a broad scope and many studies. In this study, trinary Novel metals oxide [$CuNiFe_2O_5$] nanocomposite is successfully synthesized by Uv-irradiation presses with a maximum intensity wavelength at 365 nm. The nanocomposite was investigated by scanning and transmission electron microscopy measurements (SEM and TEM), and their crystal structure is obtained by the X-ray diffraction technique (XRD). The percentage of elements on the sample was determinate by an Energy-dispersive X-ray spectroscope (EDX) and X-ray mapping. The energy gap is equal to 2.48 eV calculated by photoluminescence spectroscopy (PL). Incorporating $CuNiFe_2O_5$ NPs enhanced the uptake of Cibacron brilliant red dye (CBR). A faster CBR adsorption onto $CuNiFe_2O_5$ nanocomposite at a contact time of 75 min. The Freundlich (R2 > 0.9684) and pseudo-second-order (R2 > 0.9749) models were most appropriate in the description of the adsorption process. A thermodynamic study was performed to calculate the ΔG, ΔH, and ΔS parameters of 1.415 kJ/mol, 7.63 J/mol K, and 20.8 J/mol. Finally, the novel synthesized nanocomposite is a good adsorbate surface for Cibacron brilliant red dye.

Keywords: $CuNiFe_2O_5$ NPs, Cibacron brilliant red dye, UV-irradiation, adsorption.

1. Introduction

One of the biggest problems that a person faces in the current era is environmental pollution, the danger of which increases through various human activities, as it was found that environmental pollution has a close relationship with the population expansion in the world. [1] Water is one of the essential elements in sustaining life. Freshwater resources have recently witnessed a significant deterioration due to technological progress [2], as thousands of chemical compounds are discharged daily, directly or indirectly, to water sources without any treatment [3]. Therefore, researchers' water pollution problem has received significant attention in the modern era [1]. Organic materials are an essential part of the components of industrial wastewater. Organic pollutants are of high risk in terms of their long-term impact, as some cause cancerous diseases [4]. Dyes are considered to be organic pollutants in aqueous systems, and they include all compounds used to color textiles, leather, food, and other materials, which may cause many risks to all elements of the environment as a result of their high toxicity, especially when they are present in high concentrations [5]. Reports of the World Health Organization indicate that most of the diseases spread in developing countries are caused by contamination of drinking water. Therefore, several researchers have used several methods to treat industrial water [6,7]. Several ways have been used to treat and remove organic pollutants in industrial water. Among them are chemical oxidation, photo-oxidation, ion exchange, reverse osmosis, and adsorption method [8]. The adsorption method on hard porous surfaces is one of the methods Reports of the World Health Organization indicate that Commonly used in purifying contaminated water, many surfaces such as wood, cellulose [9], activated carbon [10-12], and others were used. Many previous studies and research in which different adsorbents were used to adsorb the cibacron brilliant red B dye [13].In this article, a compound composed of three metal oxides (ternary compounds) is abused: copper oxide, nickel oxide, and iron oxide[13]. The compound is prepared by irradiating ultraviolet light using a photovoltaic cell. Nano metal oxides CuO, NiO, and Fe_2O_3, because these oxides are environmentally friendly, have high

*Corresponding author e-mail: ahmed.rheima@yahoo.com; (Ahmed Mahdi Rheima).
Receive Date: 07 March 2021, Revise Date: 05 June 2021, Accept Date: 06 June 2021
DOI: 10.21608/ejchem.2021.66737.3437

surface efficiency (large surface area), good electrical conductivity, low toxicity, and many other characteristics [14 – 16]. And the biological activity of a variety of bacteria and can absorb these characteristics in a single case [17, 18]. Combining these oxides together in the triple superposition form of nanostructures increases even more [19,20]. The aim of this project included Test the efficacy of a photo-prepared trinary $CuNiFe_2O_5$ nanostructure in removing the Cibacron Brilliant Red B that is one of the dyes used at the Wasit Governorate textile factory, and the remainder are mostly discarded as a wastewater.

2. Experimental part

2.1 Synthesis of $CuNiFe_2O_5$ Nanocomposite

All chemicals were used purchased from (BDH) and without any purification. $CuNiFe_2O_5$ nanoparticles have been prepared by photo irradiation method, irradiation cell, as in figure 1, was used to irradiate copper nitrate, nickel nitrate, and Iron nitrate as sources of $CuNiFe_2O_5$ nanoparticles. Immersed UV source (125 W mercury medium pressure lamp) is used with maximum light intensity at 365 nm. The cell contains a quartz tube like a jacket for immersion UV source in the solution of salts. Pyrex tube is used as a reactor. An ice bath cools the reactor to avoid rising temperatures due to UV irradiation [21,22]. Accordingly, 30 ml, 0.01 mole $Cu(NO_3)_2$, 30 ml, 0.01 mole $Ni(NO_3)_2$, and 30 ml, 0.01 mole $Fe(NO_3)_3$ were mixed to gathers as a stoichiometric ratio (1:1:1). Then, 90 ml, 0.03 mole of urea is added slowly (drop per second) to the mixture and kept stirred at 30 min for 15 min. after that, the solution is irradiated by photocell for 30 min. The nanocomposite is precipitated as a red-brown (dark) powder; it is separated and washed several times with deionizing water (all steps done with centrifuge then decantation). The precipitate has dried in an oven at 100°C for 3 h and calcined at 400°C for 3 h. Black-brown color precipitate $CuNiFe_2O_5$ nanoparticles have been obtained.

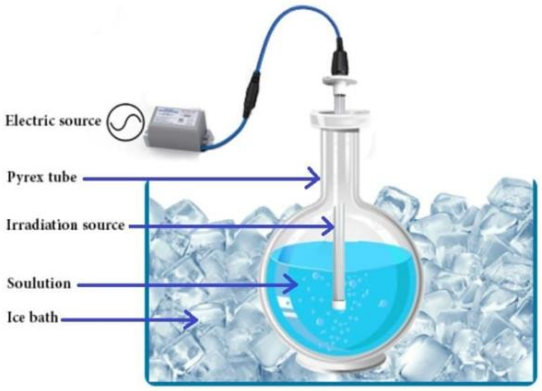

Figure .1. diagram of photolysis cell

2.2 Adsorption of Cibacron brilliant red B on $CuNiFe_2O_5$ NPs

Ten-milliliter solutions were prepared by dissolving the dye in deionized water in the standard (500 ppm) solution of cibacron brilliant red B at different concentrations between 5 and 25 ppm. The $CuNiFe_2O_5$ nanoparticles were added 0.01 g and shackled at selected temperatures at 288 K, 298 K, 308 K, 318 K, and 328 K for approximately 90 min. The following systems were filtered and used to determine the concentration of dye in the filtrate in a UV-visible absorption spectrophotometer [21-23].

$$Qe=(C_0 \_ Ce)Vsol/M \quad (1)$$

Where Qe (mg/g) is the adsorption capacity at equilibrium, C0 and Ce are concentrations of cibacron brilliant red B (mg/L) initially, and equilibrium, M is the mass of the CuNiFe2O5 nanoparticles (g). V sol is the volume of cibacron brilliant red B (L).

2.3 Characterization

Some techniques have been used to characterize the $CuNiFe_2O_5$ nanoparticles sample. X-ray diffraction (XRD) Model D-5000 was used to investigate the composition of the specimens by using Cu-Kα radiation (λ=0.154nm) source in θ/2θ. The XRD (10˚ to 80˚) and measurement temperature (25 °C) are 2$\boldsymbol{\theta}$ of $CuNiFe_2O_5$ NPS [20]. Field emission scanning electron microscope (FE-SEM) model Jeol JSM-6010LV A total of 20 µL was lowered over a grid of 300-mesh Cu and dried at room temperature. Photoluminescence measurements (PL) emission measured of $CuNiFe_2O_5$ nanoparticles to calculate the energy gap of emission. TEM model Jeol JSM-6010LV observed sample morphologies with 500 X and 60 kX magnification with a 5kV accelerating violation.TEM analyzes the sample $CuNiFe_2O_5$ nanoparticle powder discrete in the deionized and sonic water for approximately 15 minutes [21-23].

3. Results and discussion

3.1 XRD characterization of metals oxide Nanostructures

The composition of the specimen was investigated using X-ray diffraction (XRD) Model D-5000 with a Cu-K radiation (=0.154nm) source in 2Θ. Figure 2 depicts the sample's XRD patterns Before and after calcination at 400 ˚C. Before calcination in fig 2, X-ray diffraction examination of the prepared particles before the incineration showed deflection peaks at an angle of 11.71˚, 23.62˚, 36.06˚, 39.35˚ and, 61.85˚ that belong to the prepared triple hydroxide chain Fe (n)

Cu (n) Ni (n) (OH) n. After burning the model with a degree of 400 ˚C, he gave deflection values at an angle of 2θ = 35.47, 38.72, 43.39, 48.42, 61.58, 62.95, and 75.09, which refer to the $CuNiFe_2O_5$ nanoparticles, which refer to the hexagonal structure of the nanocomposite. The crystal size was determined using the Scherrer equation [21,23]. The crystal size was calculated to be approximately 15.23 nm.

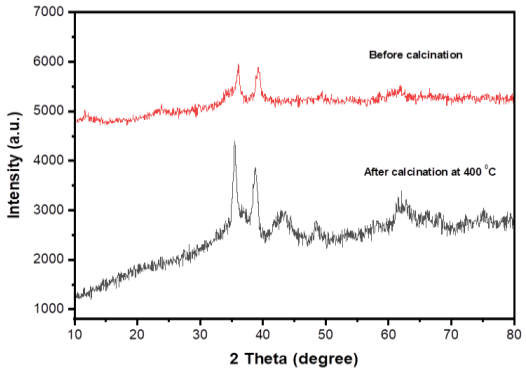

Fig.2. XRD graph of the $CuNiFe_2O_5$ nanoparticles.

3.2 FE-SEM characterization

FE-SEM was used to investigate the surface morphology of pure $CuNiFe_2O_5$ nanoparticles calcined at 400 ˚C, Fig.3. The production of semi-spherical aggregates as nearly uniform distribution for the prepared sample can be concluded from SEM analysis. The crystal nature of equal-sized synthesized nanoparticles is demonstrated. $CuNiFe_2O_5$ nanoparticles have been discovered to have an average size of 18.68 nm, and are homogeneous with little aggregation due to their small size. These findings are nearly identical to those obtained from the Typical XRD pattern.

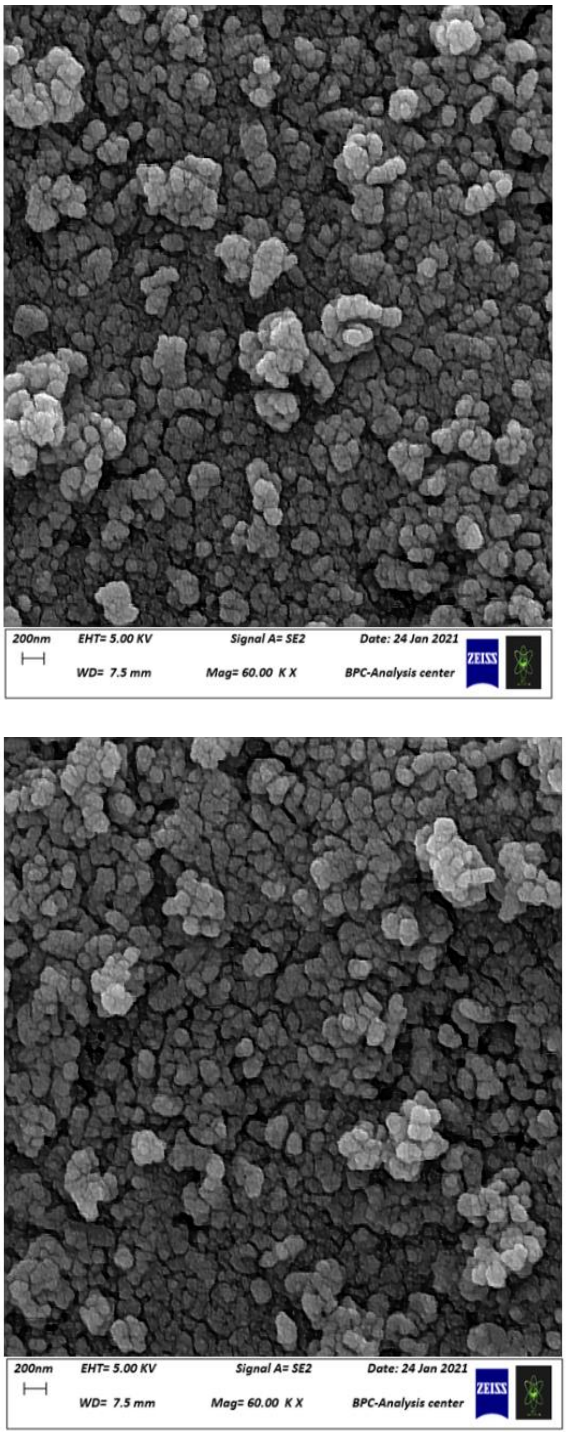

Fig.3. SEM micrographs of the $CuNiFe_2O_5$ nanoparticles.

3.3 EDX characterization

The EDX spectrum of $CuNiFe_2O_5$ nanoparticles is shown in Fig.4. Typical Iron, Nickel, Copper, and oxygen peaks are present in the spectrum. The results confirm the high purity of the synthesized

nanostructures. The theoretical calculations of the elements agree with the practical estimates obtained from the EDX measurement. Figure 5 indicates that $CuNiFe_2O_5$ NPs have been spread well by the mixed catalyst's matrix. Further data indicate typical images of x-ray mapping to display the distribution of elemental components of a CuO , NiO, and Fe_2O_3 catalyst, which will support the dispersion of the catalyst element.

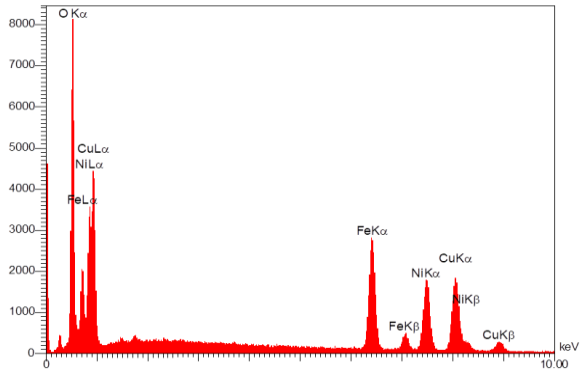

Fig.4. EDX spectrum of $CuNiFe_2O_5$ NPs.

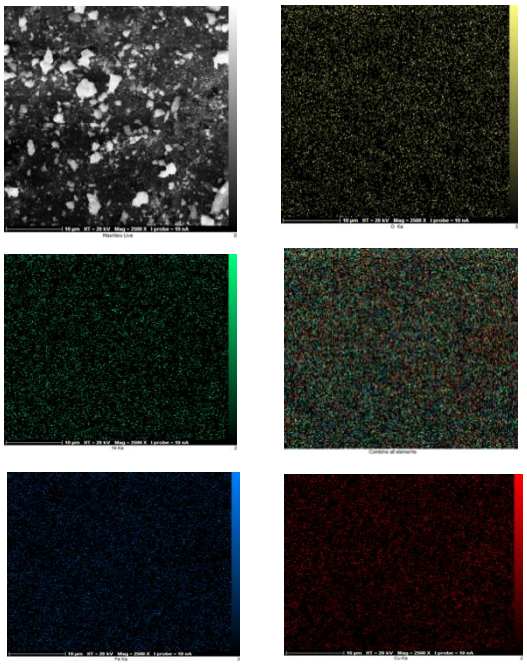

Fig.5.X-ray mapping of $CuNiFe_2O_5$NPs.

3.4 TEM spectroscopy

The TEM of $CuNiFe_2O_5$ nanoparticles is shown in Figure 6. The TEM image of nanoparticles of different shapes and sizes is shown in Figure 6. The size of the particles varied between 6 to 16 nm. The larger particles may result from smaller nanoparticles' agglomeration with dimensions that match the XRD analysis described. The crystallite size is measured with XRD based on the expansion of Bragg's reflections because of the number of parallel lattice planes causing diffraction. The Scherrer equation parameter k approximates the crystallite shape factor; however, the size distribution is not considered, resulting in size values different from the TEM.

Fig.6. TEM micrographs of the $CuNiFe_2O_5$ NPs

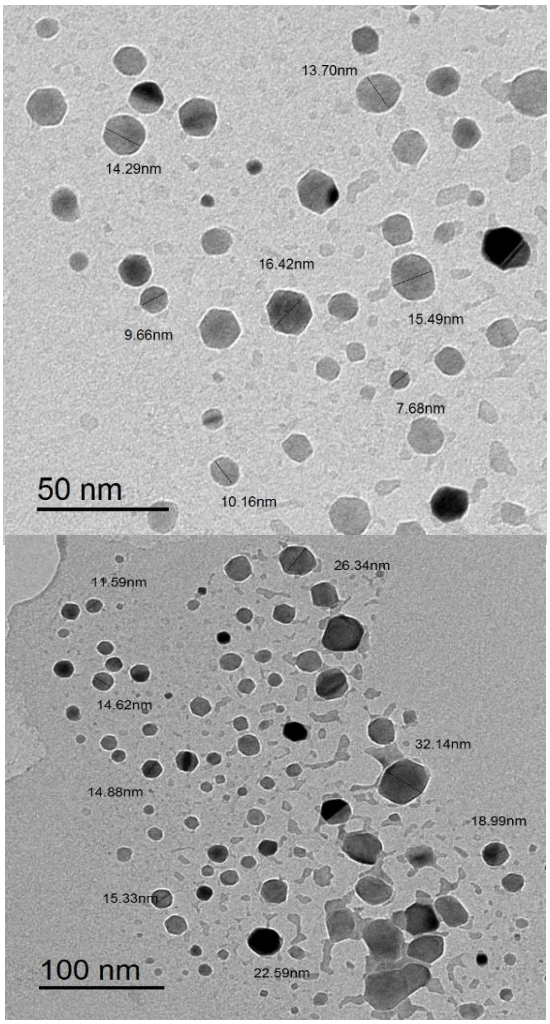

3.5 Photoluminescence measurements (PL)

Nano-powder of CuNiFe2O5 nanoparticles calcined at 400 o C were analyzed using a solid-state photo-luminescent (PL) spectrum (Perkin– Elmer spectrometer design LS55 with photomultiplier tube) for prepared its emissions. The behavior of the PL spectrum is highly influenced by the size distribution of nanoparticles, which can be derived from various sources. To measure the emission energy gap, Figure 7 shown the fluorescence spectra of CuNiFe2O5 nanoparticles with a maximum wavelength of 498 nm. The PL spectra have a single peak in this case, with a nearly wide full width at half limit (FWHM).

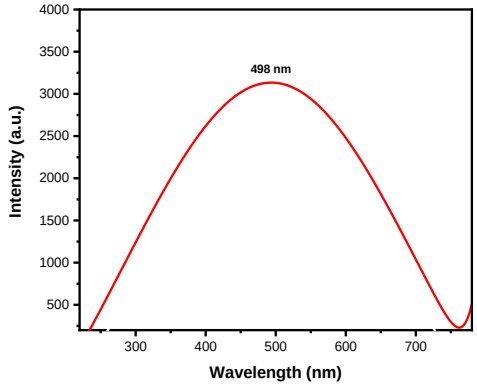

According to the equation Eg (eV) = 1240\λ [22], the energy gap was 2.48 ev .

Adsorption isotherms

The main stage in the adsorption analysis is to adjust the adsorption isotherm to the adsorption results to establish the interaction of the adsorption and the dye interact. The Freundlich and Langmuir models were considered in this work. In the following formula is shown the linear process of Freundlich adsorption [21-24]:

$$\log(Qe) = \log(kf) + (\frac{1}{n}) \log(Ce) \qquad (2)$$

Kf and n are called Freundlich constants, representing adsorption capacity and adsorption intensity, respectively. As shown in Figure 8, The kf is recorded from the intercept, and n is recorded from the slope (0.832). This result is consistent with the proven physical adsorption [25]. The adsorption is more fitted with Freundlich isotherm model (R^2=0.968).

Fig.7. The PL analysis of $CuNiFe_2O_5$ NPs.

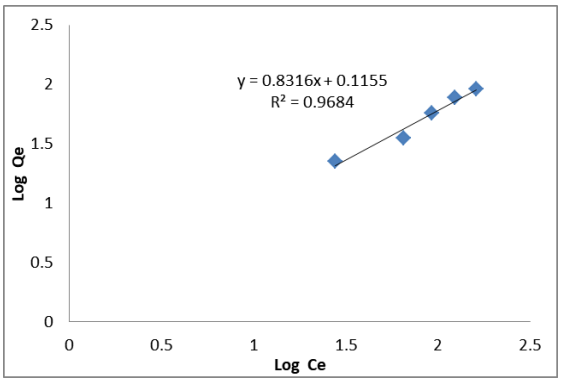

Fig.8. the Freundlich isotherm model plot at 298 K.

The data conforms to the Langmuir adsorption isotherm, as seen in the following formulation, [23-26]:

$$Ce/Qe=1/(qmax)\ Kl+ Ce/(qmax)\text{------}(3)$$

KL (mg/L) is the Langmuir constant, and q max (mg/g) is the maximum amount of d cibacron brilliant red B. The dimensionless constant (RL) is also referred to as the separation factor that indicates and

$$Rl=1/(1+KlCi)\ \text{----}(4)$$

Ci (mg / L) is the initial concentration of the dye, and the RL values are all within the range of (0-1), which indicates that the dye has better adsorption on $CuNiFe_2O_5$ NP as shown in Figure 9.

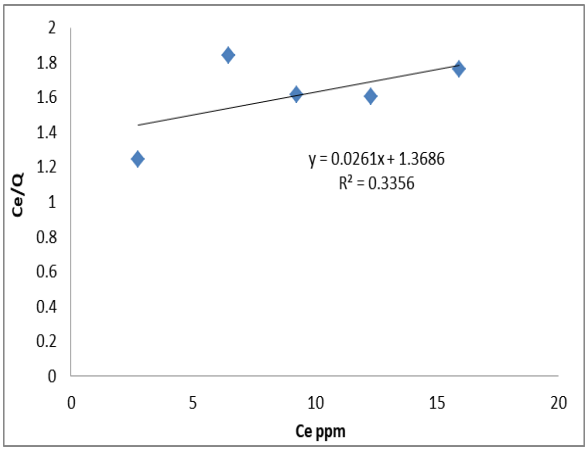

Fig.9. The Langmuir isotherm model at 298 K.

- Effect of contact time

In a series of experiments, 0,01 g $CuNiFe_2O_5$ NPs with 10mL dye (10 ppm) was used to measure contact time to reach equilibrium time. At 200 rpm,

the mixture was shaken at 298 K. At the beginning of 30-45 minutes, adsorption is very rapid. The rapid adsorption comes from the strong bond between the active $CuNiFe_2O_5$ nanoparticles and the dye. Due to the surface of the nanoparticles, the adsorption rate of the dye becomes a constant value after 75 minutes, as shown in Figure 10.

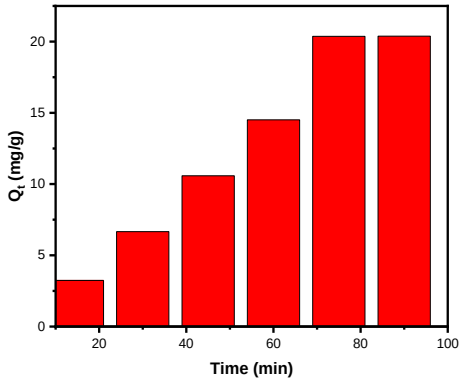

Fig.10. Effect of time on adsorption of dye onto the $CuNiFe_2O_5$ NPs.

- Effect of adsorbent mass

The adsorbent efficiency was founded by adding various quantities of $CuNiFe_2O_5$ NPs (0.01 g, 0.05 g, 0.1 g and 0.15 g) to 10 ppm of dye. At 200 rpm, the mixture was shaken at 298 K. The relationship between adsorption amount and mass is shown in the graph. First, due to the increase of active sites in nanocomposites, the adsorption speed is very fast. The rise in dye adsorption is shown in Figure 11. By increasing the quantity of $CuNiFe_2O_5$ NPs mass.

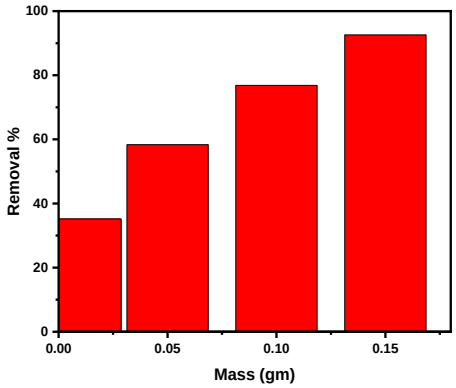

Fig.11. Effect of adsorbent mass on adsorption of dye onto the $CuNiFe_2O_5$ NPs**.**

- **Effect of Temperature**

The temperature impact of dye adsorption on the $CuNiFe_2O_5$ NP surface was studied at selected temperatures at 288K, 298 K, 308 K, 318 K, and 328 K [27,28]. With the rising temperature, the amount of dye adsorption solution increases. This results in the endothermic process, and the average value of ΔH° is positive. This demonstrates the mechanism of absorption and adsorption. As temperature increases, the diffusion molecules are absorbed in the holes, the rate of diffusion increases, and the strong bond is associated with the adsorbent. Thermodynamic parameters provide accurate data on adsorption-related changes in the inherent energy and should be evaluated appropriately. In this analysis, the following equations were used to measure the following adjustments to predict the mechanism of adsorption by using the free energy of adsorption (ΔG°), entropy (ΔS°) and enthalpy (ΔH°) [23-28]:

$$\ln(Ke) = \frac{-\Delta H}{RT} + \frac{\Delta S}{R} \quad \text{----------(5)}$$

$$Ke = Qe/Ce \quad \text{---------(6)}$$

$$\Delta G = \Delta H \_ T\Delta S \quad \text{---------(7)}$$

R is 8.314 J/mol K (gas constant), Ke is equilibrium constant, and T is the temperature in Kelvin (K). As a van't Hoff plot between ln K and 1/T in Fig.12, The ΔH was 7.630514 kJ/mole determent by slope, which showed the interaction was endothermic. The ΔS from the intercept were 20.8 J/mole that showed the adsorbed particles were as yet in steady movement on a superficial level. They were absorption and adsorption. . The positive ΔG value is equal to 1.415 KJ/mole at 298 K, which implies non-spontaneous adsorption.

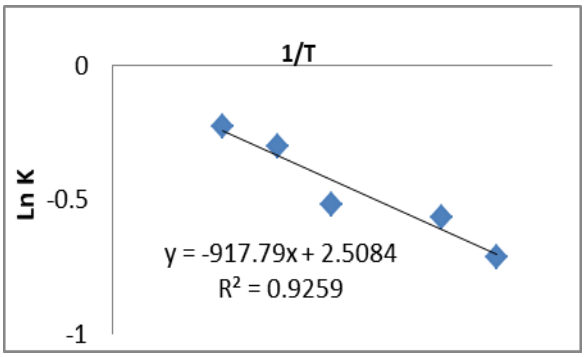

Fig.12. the van't Hoff plot between ln K and 1/T.

- Dynamics

The adsorption dynamics of dye on the surface adsorbents of $CuNiFe_2O_5$ NPs are crucial in adsorbent applications. The dye study found the adsorption equilibrium time was around 75 min for 0.01 g of the nanocomposite adsorbents. Furthermore, classical and kinetic models in this study were used to portray the information of adsorption mentioned above as follows:

Pseudo-first-order model [23, 29]:

$$\ln(qe - qt) = \ln(qe) - k1\, t \qquad \text{-------(8)}$$

Where qe (mg g -1) is the adsorption capacity at equilibrium, qt (mg g -1) is the adsorbed amount of dye after time t (min), and k1 is the pseudo-first-order rate constant (min-1) and as shown in Fig.13.

The pseudo-second-order kinetic model can be expressed as [23, 30]:

$$\frac{1}{qt} = \frac{1}{k2\, qe} + \frac{t}{qe} \qquad \text{---------- (9)}$$

Where k2 is the pseudo-second-order rate constant, the pseudo-second-order model with a high association factor (R2 > 0.9749) can properly describe the kinetic information, Fig. 14.

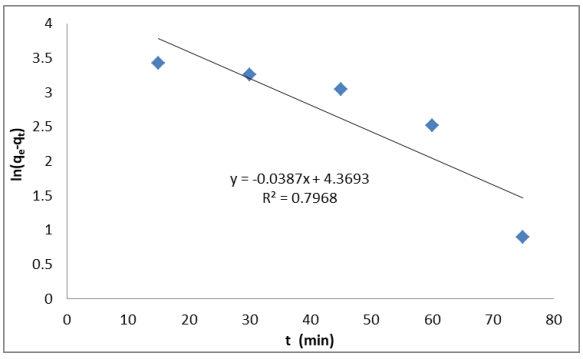

Fig.13. Dynamic of adsorption of dye pseudo-first-order.

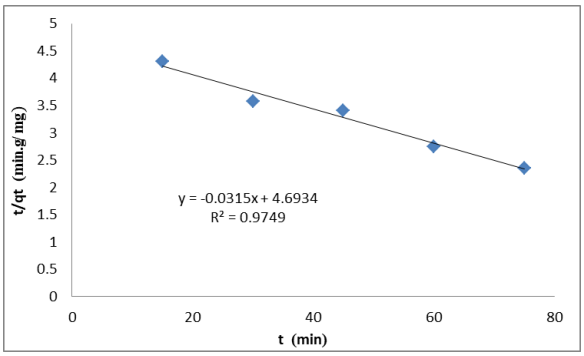

Fig.14. Dynamic of adsorption of dye pseudo-second-order.

4. Conclusion

In conclusion, high-quality $CuNiFe_2O_5$ NPs were made by photochemical technique following XRD, SEM/EDX, PL, and TEM imaging. The range particulate size of $CuNiFe_2O_5$ NPs was 6 to 16 nm, estimated by TEM. The adsorption properties shown are excellent for eliminating dye from watery solutions. Both kinetic and thermodynamic studies demonstrated the efficiency of $CuNiFe_2O_5$ NPs adsorption. Freundlich and Langmuir isotherm models were well suited for the results. The adsorption is more fitted with Freundlich isotherm model. The thermodynamic indicate that the adsorption is endothermic and nonspontaneous. The enthalpy value (7.630514 kJ/mole) was calculated by the slope of the van't Hoff plot, which indicates the physical properties of adsorption. The pseudo-second-order with R2 = 0.9749 conformity to this adsorption.

Conflict of interest

The authors not have any conflict of interest

5. References

[1] Rheima AM, Mohammed MA, Jaber SH, Hameed SA. Adsorption of selenium (Se4+) ions pollution by pure rutile titanium dioxide nanosheets

electrochemically synthesized. Desalination and Water Treatment. 2020 Aug 1;194(2020):187-93.

[2] Rheima AM, Mahmood RS, Hussain DH, Abbas ZS. Study the Adsorption Ability of Alizarin Red Dye From Their Aqueous Solution on Synthesized Carbon Nanotubes. Digest Journal of Nanomaterials and Biostructures. 2020;15(4).

[3] Abouda NA, Jasima BE, Rheimab AM. Methylene Orange dye removal in aqueous solution using synthesized CdO-MnO2 nanocomposite: kinetic and thermodynamic studies. Chalcogenide Letters. 2021 May 1;18(5):237-43

[4] Ismail AH, Al-Bairmani HK. Nano-synthesis, spectroscopic characterisation and antibacterial activity of some metal complexes derived from Theophylline. Egyptian Journal of Chemistry. 2020 Dec 1;63(12):4951-62

[5] Ismail AH, Al-Bairmani HK, Abbas ZS, Rheima AM. Synthesis, Characterization, Spectroscopic and Biological Studies of Zn (II), Mn (II) and Fe (II) Theophylline Complexes in Nanoscale. Nano Biomed. Eng. 2020 Jul 1;12(3):253-61.

[6] Rheima AM, Anber AA, Abdullah HI, Ismail AH. Synthesis of Alpha-Gamma Aluminum Oxide Nanocomposite via Electrochemical Method for Antibacterial Activity. Nano Biomed. Eng. 2021;13(1):1-5.

[7] Saleh, I.A., Zouari, N. and Al-Ghouti, M.A., 2020. Removal of pesticides from water and wastewater: Chemical, physical and biological treatment approaches. Environmental Technology & Innovation, p.101026.

[8] Rheima, A.M., Mohammed, M.A., Jaber, S.H. and Hameed, S.A., 2019. Synthesis of silver nanoparticles using the UV-irradiation technique in an antibacterial application. Journal of Southwest Jiaotong University, 54(5).

[9] Rheima AM, Aboud NA, Jasim BE, Ismail AH, Abbas ZS. Synthesis and structural characterization of ZnTiO3 nanoparticles via modification sol-gel prosses for assessment of their antimicrobial activity. International journal of pharmaceutical research. 2021 Jan;13(1).

[10] Kadhum HA, Salih WM, Rheima AM. Improved PSi/c-Si and Ga/PSi/c-Si nanostructures dependent solar cell efficiency. Applied Physics A. 2020 Oct;126(10):1-5.

[11] Rheima, A.M., Hussain, D.H. and Abed, H.J., 2020, November. Fabrication of a new photo-sensitized solar cell using TiO2\ZnO Nanocomposite synthesized via a modified sol-gel Technique. In IOP Conference Series: Materials Science and Engineering (Vol. 928, No. 5, p. 052036). IOP Publishing.

[12] Aboud, N.A.A., Alkayat, W.M., Hussain, D.H. and Rheima, A.M., 2020, November. A comparative study of ZnO, CuO and a binary mixture of ZnO0. 5-CuO0. 5 with nano-dye on the efficiency of the dye-sensitized solar cell. In Journal of Physics: Conference Series (Vol. 1664, No. 1, p. 012094). IOP Publishing

[13] Kamil AF, Abdullah HI, Rheima AM, Mohammed SH. Photochemical synthesized NiO nanoparticles based dye-sensitized solar cells: a comparative study on the counter electrodes and dye-sensitized concentrations. Journal of Ovonic Research. Vol. 17, No. 3, May - June 2021

[14] Kamil AF, Abdullah HI, Rheima AM, Khamis WM. Modification of hummers presses for synthesis graphene oxide nano-sheets and graphene oxide/Ag nanocomposites. Journal of Ovonic Research. 2021 May 1;17(3).

[15] Ali AA, Al-Hassani RM, Hussain DH, Rheima AM, Meteab HS. Synthesis, spectroscopic, characterization, pharmacological evaluation, and cytotoxicity assays of novel nano and micro scale of copper (II) complexes against human breast cancer cells. Drug Invention Today. 2020 Jan 15;14(1).

[16] Ismail AH, Al-Bairmani HK, Abbas ZS, Rheima AM. Nanoscale synthesis of metal (II) theophylline complexes and assessment of their biological activity. Nano Biomed. Eng. 2020 Apr 1;12(2):139-47.

[17] Rheima AM, Mohammed MA, Jaber SH, Hasan MH. Inhibition effect of silver-calcium nanocomposite on alanine transaminase enzyme activity in human serum of Iraqi patients with chronic liver disease. Drug Invention Today. 2019 Nov 15;12(11):2818-21.

[18] A.H. Ismail, H.K. Al-Bairmani, Z.S. Abbas, A.M. Rheima. Nano metal-complexes of theophylline derivative: synthesis, characterization, molecular structure studies, and antibacterial activity. In IOP Conference Series: Materials Science and

Engineering 2020 Nov 1 (Vol. 928, No. 5, p. 052028). IOP Publishing

[19] Aboud NA, Jasim BE, Rheima AM. Adsorption study of phosphate ions pollution in aqueous solutions using microwave synthesized magnesium oxide nanoparticles. Digest Journal of Nanomaterials and Biostructures. 2021;16(3).

[20] Salman AT, Ismail AH, Rheima AM, Abd AN, Habubi NF, Abbas ZS. Nano-Synthesis, characterization and spectroscopic Studies of chromium (III) complex derived from new quinoline-2-one for solar cell fabrication. InJournal of Physics: Conference Series 2021 Mar 1 (Vol. 1853, No. 1, p. 012021). IOP Publishing.

[21] Rheima, A., Anber, A.A., Shakir, A., Salah Hammed, A. and Hameed, S., 2020. Novel method to synthesis nickel oxide nanoparticles for antibacterial activity. Iranian Journal of Physics Research, 20(3), pp.51-55.

[22] Mohammed, M.A., Rheima, A.M., Jaber, S.H. and Hameed, S.A., 2020. The removal of zinc ions from their aqueous solutions by Cr2O3 nanoparticles synthesized via the UV-irradiation method. Egyptian Journal of Chemistry, 63(2), pp.425-431.

[23] Hussain DH, Rheima AM, Jaber SH. Cadmium ions pollution treatments in aqueous solution using electrochemically synthesized gamma aluminum oxide nanoparticles with DFT study. Egyptian Journal of Chemistry. 2020 Feb 1;63(2):417-24.

[24] Safri, A., Fletcher, A.J., Abdel-Halim, E., Ismail, M.A. and Hashem, A., 2020. Calligonum crinitum as a novel sorbent for sorption of Pb (II) from aqueous solutions: thermodynamics, kinetics, and isotherms. Journal of Polymers and the Environment, pp.1-11.

[25] Lima, E.C., Gomes, A.A. and Tran, H.N., 2020. Comparison of the nonlinear and linear forms of the van't Hoff equation for calculation of adsorption thermodynamic parameters (Δ S° andΔ H°). Journal of Molecular Liquids, 311, p.113315.

[26] Wu, W., Lu, C., Yuan, M., Tian, Y. and Zhou, H., 2021. Acidification of potassium bismuthate for enhanced visible-light photocatalytic degradation ability: an effective strategy for regulating the abilities of adsorption, oxidation, and photocatalysis. Applied Surface Science, p.148873.

[27] Zulfiqar, M., Chowdhury, S., Samsudin, M.F.R., Siyal, A.A., Omar, A.A., Ahmad, T. and Sufian, S., 2020. Effect of organic solvents on the growth of TiO2 nanotubes: An insight into photocatalytic degradation and adsorption studies. Journal of Water Process Engineering, 37, p.101491.

[28] Satilmis, B., 2020. Amidoxime modified polymers of intrinsic microporosity (PIM-1); a versatile adsorbent for efficient removal of charged dyes; equilibrium, kinetic and thermodynamic studies. Journal of Polymers and the Environment, 28(3), pp.995-1009.

[29] Ezzati, R., 2020. Derivation of pseudo-first-order, pseudo-second-order and modified pseudo-first-order rate equations from Langmuir and Freundlich isotherms for adsorption. Chemical Engineering Journal, 392, p.123705.

[30] Regazzoni, A.E., 2020. Adsorption kinetics at solid/aqueous solution interfaces: on the boundaries of the pseudo-second order rate equation. Colloids and Surfaces A: Physicochemical and Engineering Aspects, 585, p.124093.